

Digital Active Nulling for Frequency-Multiplexed Bolometer Readout: Performance and Latency

Graeme Smecher^a, Tijmen de Haan^b, Matt Dobbs^c, and Joshua Montgomery^d

^aThree-Speed Logic, Victoria, Canada

^bHigh Energy Accelerator Research Organization (KEK), Tsukuba, Japan

^{c,d}McGill University, Québec, Canada

ABSTRACT

We consider the stability and performance of a discrete-time control loop used as a dynamic nuller in the presence of a relatively large time delay in its feedback path.

Controllers of this form occur in mm-wave telescopes using frequency-multiplexed Transition Edge Sensor (TES) bolometers. In this application, negative feedback is needed to linearize a Superconducting Quantum Interference Device (SQUID) used as an amplifier. M such feedback loops are frequency-multiplexed through a SQUID at distinct narrowband frequencies in the MHz region. Loop latencies stem from the use of polyphase filter bank (PFB) up- and down-converters and have grown significantly as the detector count in these experiments increases.

As expected, latency places constraints on the overall gain K for which the loop is stable. However, latency also creates spectral peaks at stable gains in the spectral response of the closed loop. Near these peaks, the feedback loop amplifies (rather than suppresses) input signals at its summing junction, rendering it unsuitable for nulling over a range of stable gains.

We establish a critical gain K_C above which this amplifying or “anti-nulling” behaviour emerges, and find that K_C is approximately a factor of 3.8 below the gain at which the system becomes unstable.

Finally, we describe an alteration to the loop tuning algorithm that selects an appropriate (stable, effective for nulling) loop gain without sensitivity to variations in analog gains due to component tolerances.

Keywords: Negative Feedback, Delays, Closed-Loop Systems, Stability Analysis

1. INTRODUCTION

At the South Pole Telescope in Antarctica,¹ and in many other mm-wave telescopes,^{2–7} frequency-multiplexed transition edge sensor (TES) bolometers convert incident radiation power into an electrical signal for measurement. TES bolometers achieve extremely high sensitivity by operating near their superconducting transition temperatures, where their resistance varies strongly with temperature (and hence, absorbed radiation).⁸

To further amplify faint astrophysical signals for digitization by room-temperature electronics, these telescopes use cryogenic superconducting quantum interference devices (SQUIDs). SQUIDs are magnetometers that, when coupled to an input coil, form exquisitely sensitive transimpedance amplifiers. However, SQUIDs in this configuration exhibit a nonlinear (approximately sinusoidal) response to input current. To linearize SQUIDs, their input signals are typically DC biased with a limited dynamic range to avoid distortion.

In a frequency-multiplexed readout,^{9,10} each SQUID amplifies signals from M bolometers at distinct carrier frequencies in the MHz range. Designs supporting values of M between 8 and 128 have been fielded, and future mm-wave telescopes are expected to continue aggressive growth of the multiplexing factor M .

In Ref. 11, we introduced Digital Active Nulling (DAN), a mechanism for adaptively nulling the input to a cryogenic SQUID amplifier. DAN linearizes a SQUID in the presence of multiple narrow-band modulated carriers by dynamically controlling the amplitude of a nulling tone associated with each carrier. DAN also reduces the

E-mail: gsmecher@threespeedlogic.com

effective input impedance of the SQUID inductor in the bands surrounding each detector, reducing the impact of parasitic circuit elements in the cold electronics that can compromise detector stability and response linearity. A DAN system forms multiple frequency-multiplexed feedback loops with a single cryogenic summing junction at the SQUID input coil. Although each DAN loop operates at RF, its negative feedback operates at baseband in a small frequency range around each carrier, and the loop bandwidth is as small as several kHz.

DAN has been successfully deployed on several mm-wave telescopes since its introduction,^{2,4,6,7,12} and though the means of implementing this signal path has evolved,¹ the underlying nulling algorithm has not.

This work investigates DAN dynamic performance and loop stability, focusing primarily on the impact of latency (a design parameter driven higher by the efficient design of high-channel-count up- and down-converters) and loop gain (a tunable parameter that determines nulling efficiency and spectral flatness across the bolometer bandwidth). As the detector count of mm-wave telescopes continues to increase, the relationship between these performance characteristics and the maximum attainable M is increasingly important.

This paper is organized as follows:

- We describe a frequency-multiplexed bolometer readout system operating in DAN mode, to provide both a theoretical foundation and a motivating example for the remainder;
- We reduce the system to a simplified model of the DAN feedback loop at baseband, and investigate the system’s stability under varying latency and loop gain;
- We investigate the system’s suitability as a nulling loop for SQUID amplifiers, and impose further loop gain constraints to prevent unwanted amplification of signals at the input to the SQUID; finally,
- We describe alterations to the tuning algorithm that allow nearly optimal selection of the loop gain, even when the analog gains are only approximately known (e.g. perturbations due to component variations).

2. FREQUENCY-MULTIPLEXED BOLOMETER READOUT

2.1 Cryogenic Electronics

The cryogenic electronics associated with a frequency-multiplexed bolometer readout system are shown in Figure 1. Incident millimeter-wave energy is absorbed by an array of M focal-plane bolometers associated with a single SQUID, each of which acts as a time-varying resistance $R_1(t), R_2(t), \dots R_M(t) \approx 1 \Omega$. Typical multiplexing factors range between $M = 16$ and $M = 128$. (The design of the cryogenic electronics evolves semi-independently from the warm readout electronics; see e.g. Ref. 13.)

Each bolometer is paired with a tuned LC circuit, associating that bolometer with a single carrier frequency within a comb $C(t)$ of synthesized carriers. As each bolometer’s resistance changes, the associated carrier tone is amplitude modulated to produce sidebands that encode the incident sky signal.

The modulated carrier tones are summed through an inductor L_{SQUID} . The resulting magnetic field is converted to a voltage signal by the SQUID, then amplified and digitized in room-temperature electronics.

The time scale of varying bolometer resistances (hence, the bandwidth of their associated sidebands) is determined by the dynamic characteristics of the incident mm-wave signal, which depends on the sky itself, noise contamination from thermal, optical, or electric sources, the telescope’s scanning speed, and the impact of any modulating elements such as a rotating half-wave plate used in the system. This time scale is fundamentally limited by the bolometers’ thermal time constants, which are typically in the millisecond range. Generally, the science signals of interest are captured in several tens of Hz surrounding each carrier.

To reduce the dynamic range seen by the SQUID and associated electronics, an auxiliary DAC cancels or “nulls” bolometer current at the SQUID using the signal $N(t)$ (see Figure 1). It is the primary task of the DAN loop to generate this nulling signal. The DAN loop also creates a virtual ground at the L_{SQUID} input, dramatically reducing the effective input impedance of the SQUID inductor.

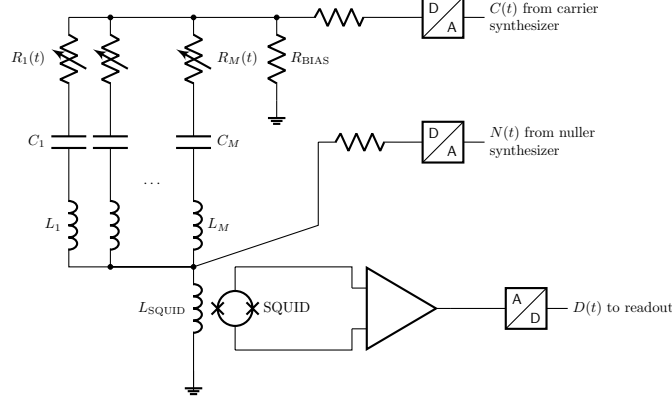


Figure 1. A simplified schematic of the analog portion of a voltage-biased, frequency-multiplexed bolometer readout system. A carrier D/A converter (top right) delivers a comb of sinusoids $C(t)$ to a bias resistance $R_{\text{BIAS}} \ll R_m(t)$, $1 \leq m \leq M$, establishing a voltage bias across M RLC networks. In these networks, the time-varying resistances $R_m(t)$ are electrical models of the bolometers. Each LC filter selects a single frequency from the carrier comb, maintaining a distinct bias carrier across each bolometer. This bias holds the bolometer in electrothermal feedback.⁸ The SQUID provides a measurement of the summed current through all M bolometers, which is cancelled by a dedicated nuller D/A converter (centre right). The residual signal is amplified and digitized for readout.

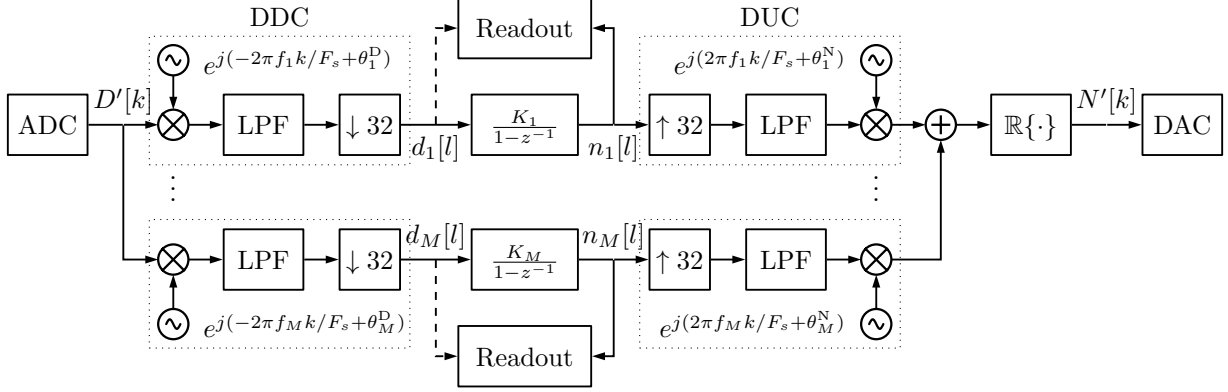


Figure 2. A representative model of the readout and nuller signal path at RF, neglecting implementation-specific latency imposed by the DUC/DDCs. The SQUID output, after amplification and digitization by the ADC (left), is presented to an array of complex downconverters with distinct frequencies f_m and phases θ_m^{D} . These signals are decimated to a lower sampling rate (from 20 MSPS to 625 kSPS), where each signal is presented to a distinct integral controller with per-channel loop gain K_m . Each integrator's output is then upconverted back to RF, and the results are summed and presented to the nuller DAC (right); see Equation (1). Science data may be selected from the open-loop demodulator path $d_m[l]$ or closed-loop nuller path $n_m[l]$, and is separately decimated and streamed for offline analysis.

2.2 Digital Signal Path

The digital signal path, shown in Figure 2, is responsible for three tasks:

- Synthesizing carrier and nuller combs for the DACs,
- Demodulating, decimating, packaging, and streaming bolometer data for analysis, and
- Using demodulator data to update the synthesizer coefficients used for nulling.

The carrier and nuller signals, which are discrete-time versions of $C(t)$ and $N(t)$, are of the form:

$$C'[k] = \mathbb{R} \left\{ \sum_{m=1}^M C_m e^{2\pi j f_m k / F_s + j \theta_m^{\text{C}}} \right\} \quad (1)$$

$$N'[k] = \mathbb{R} \left\{ \sum_{m=1}^M n'_m[k] e^{2\pi j f_m k / F_s + j \theta_m^C} \right\} \quad (2)$$

where the signal $n'_m[k]$ is an oversampled version of the baseband nuller signal $n_m[l]$ shown in Figure 2. Since the specific implementation of the digital up- and down-converters is not the subject of the present investigation, we leave the exact relationship between the high-sampling-rate signals $D'[k]$, $n'_m[k]$, and $N'[k]$ and their baseband counterparts $d_m[l]$ and $n_m[l]$ unspecified here.

Although Figure 2 does not show the carrier synthesizer path, it is a degenerate version of the nuller up-converter using programmable but constant amplitude and phase parameters C_m and θ_m^C . For the purposes of evaluating DAN loop performance, the carrier signal is stimulus and hence not relevant to stability.

In practice, implementing the digital upconverters (DUCs) and digital downconverters (DDCs) as implied by Figure 2 and Equations (1) and (2) is not computationally efficient (and hence, not power- or resource-efficient).¹⁰ Rather than implement independent up-/down-converters for each bolometer, we use intermediate up- and down-conversion stages using polyphase filter-bank (PFB) techniques.¹⁴ We also do not synthesize (and then discard) the imaginary portion of the carrier and nuller signals. In exchange for a more efficient implementation, the use of PFB techniques imposes relatively high latency on the up- and downconversion chains.

Signal path designs to date have exhibited combined nuller and demodulator latencies between 5 μ s and 31 μ s; the current signal path design has a combined nuller and demodulator latency of approximately $\tau \approx 14 \mu$ s.

The specific implementation of the DDC and DUC blocks are not the subject of the present investigation; here, only the latency term τ is important. We will return to the latency term after describing how such a system is tuned in practice.

2.3 Tuning and Operation

The signal path in Figure 2 and the signals in Equations (1) and (2) have many parameters (carrier gains, phases, loop gains, and frequencies). To motivate how and when these parameters are selected, a simplified description of a typical array tuning algorithm follows.

1. The array starts off at a temperature above the bolometers' superconducting transition T_c (typically 4 K, the temperature of the cryostat's liquid Helium bath); hence, bolometers exhibit a nominal resistance regardless of any optical power absorbed or electrical power dissipated. Signal-path frequencies f_m are programmed using a database of pre-characterized parameters. Amplitude settings (C_m, K_m) ensure $C(t) = N(t) = 0$. Data readout uses the open-loop (dashed) path in Figure 2.
2. The readout phases θ_m^D are tuned to rotate each bolometer's nuller signal into the in-phase or I component of the corresponding complex readout signal $d_m[l]$, with an 180° phase shift to ensure negative feedback.
3. The DAN loop can now be closed. To do this, nonzero gain terms K_m are programmed. Nullers begin to respond dynamically. Capture of science data is shifted from open-loop paths (the dashed lines in Figure 2) to closed-loop paths (solid lines).
4. Carrier amplitudes C_m are programmed, delivering enough electrical power to each bolometer to prevent it from latching in its superconducting state when the array is cooled below T_c . Specific C_m values are taken from a database of pre-characterized parameters.
5. The array is now cooled below the T_c of the bolometers using a sub-Kelvin refrigerator. Bolometers are now held in electrothermal feedback;⁸ the current flowing through them is a strong function of incident optical power.
6. Carrier phases θ_m^C are now tuned into the I component of the readout signal. Since the sidebands generated by optical modulation are symmetric, the science signal is entirely present in I; the Q channel may be kept for diagnostic purposes or discarded.

At this point, the detector array and readout signal path are ready to capture science data. However, the tuning process required values for the M DAN gains K_m , and we have not provided a physical or conceptual basis for the choice of these parameters.

In the remainder of this paper we establish the criteria for choosing a suitable DAN gain that is both bounded-input-bounded-output (BIBO) stable and effective at nulling the SQUID input.

3. THE SIMPLIFIED DAN LOOP

A complete model of the feedback loop and surrounding system would include both the analog system described in Figure 1 and the digital system described in Figure 2. Such a model would be comprehensive, but would prevent a convenient stability analysis. To find a tractable model of the DAN loop, we begin with some simplifying assumptions.

Since the LC combs (and indeed, the bolometers themselves) are part of the carrier path and do not form part of the feedback loop, they can be removed when considering loop stability and performance. To do so, we consider the feedback loop's input to be current injected into the inductance L_{SQUID} .*

We assume that DAN loops are adequately spaced in frequency and do not interact. This permits us to decompose the system into M individual DAN loops, and analyze the stability and performance of just one.

We assume that all RF components in the system are wideband relative to the bandwidth of the digital loop. (In current designs, operates at a sampling rate of 625 kHz and has meaningful gain only at a small fraction of this bandwidth.) These frequency-dependent terms are replaced with constant gains.

We recognize that the analog system is now frequency-independent. Gains can be freely moved across the downconverter to baseband. The DAC and ADC cancel each other out (any time delays removed by this cancellation are minor but can be re-injected using the latency model added next), followed by cancellation of the upconverter and downconverter under the assumption that the phase terms θ_m^N and θ_m^D are aligned during tuning as described above. The entire model is now discrete-time and operates at baseband.

Finally, we need to inject a latency model. Because the system is now fully discrete-time, It makes sense to do this in the z -domain where delays in integer sample counts are convenient. We add a delay of L samples in the feedback path. In our system, a latency of $\tau \approx 14 \mu\text{s}$ is equivalent to $L = 9$ at a baseband sampling rate of 625 kHz.

After these simplifications, a single DAN loop may be modelled as shown in Figure 3.

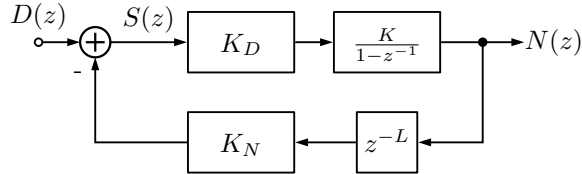


Figure 3. A model of the DAN feedback loop at baseband

This model includes the SQUID (summing junction), gains for the nuller (K_N) and demodulator (K_D) circuitry, the DAN integrator transfer function, and the latency term z^{-L} .

The closed-loop transfer function of this system at baseband is

$$H(z) = \frac{N(z)}{D(z)} = \frac{K_D K}{1 - z^{-1} + K_D K_N K z^{-L}} = \frac{K_D K}{1 - z^{-1} + K_0 z^{-L}} \quad (3)$$

*In reality, the impedances of the carrier RLC networks are non-negligible relative to the SQUID input impedance, so some nuller current intended for the SQUID coil inevitably flows back into the associated bolometer. Although this parasitic effect is critical when designing the cold electronics, it requires a separate treatment and does not impact the selection of K_m ; hence, we neglect it for the present discussion.

The transfer function from baseband input to the residual (nulled) signal seen by the SQUID is

$$E(z) = \frac{S(z)}{D(z)} = \frac{1 - z^{-1}}{1 - z^{-1} + K_N K_D K z^{-L}} = \frac{1 - z^{-1}}{1 - z^{-1} + K_0 z^{-L}} \quad (4)$$

where in both equations we have defined the combined gain $K_0 = K_N K_D K$.

3.1 Stability

Our first consideration is given to stability. This system is stable when its z -plane poles are within the unit circle; hence, we are interested in the impact of gain K_0 and latency L on the poles of $H(z)$.

Both the closed-loop and residual transfer functions have the same characteristic equation (i.e. where the denominator of the transfer function equals 0):

$$z^L - z^{L-1} + K_0 = 0 \quad (5)$$

As this equation is not soluble in closed form for typical L , we resort to numerical techniques. We show some results for stability versus latency and loop gain later (see Figure 6). As expected, loop stability diminishes with increasing K_0 and L .

For the remainder of this paper we are only interested in the performance of stable loop configurations. We now consider nulling performance within the stable regime.

3.2 Nulling Performance

Figure 4 shows the open-loop magnitude, closed-loop magnitude $H(z)$, and residual magnitude $E(z)$ versus frequency as the gain K_0 is varied. All gains in this range are stable for $L = 9$. However, at higher K_0 , there are regions where the magnitude response of the nuller loop is greater than 0 dB (that is, $|E(e^{j\omega})|^2 > 1$). Though stable, loop gains with this characteristic are not suitable for nulling because they amplify rather than suppress some inputs at the SQUID.

Similarly, Figure 5 shows the transfer functions $H(z)$ and $E(z)$ for varying latency L under a constant gain $K_0 = 0.1$. Unlike loop gain K_0 , latency is essentially a design parameter; by varying L we are exploring the performance available to a system with that latency. Stable designs with sufficiently high L also begin to exhibit anti-nulling behaviour.

Correct interpretation of these peaks is crucial. Let us suppose we are operating a DAN loop at a sufficient gain K_0 that the peak in these plots is present. Since this is a stable feedback loop, this system (both $H(z)$ and $E(z)$) does not *create* signals at these frequencies – but any signals already present within this region are amplified before being presented to the SQUID (in the case of $E(z)$) or synthesized by the nuller (in the case of $H(z)$). In practice, a signal in this region could be injected into the DAN loop from several sources:

- The signal could come from a predictable noise feature (e.g. from amplifiers in the carrier, nuller, or demodulator chain, or from the noise floor of the DACs, ADCs, or digital signal chain).
- The signal could come from a neighbouring bolometer. (This is unlikely, since in practice bolometer LCs are spaced much further apart than the spectral peaks at approximately 10 kHz in these design examples.)
- The signal could come from EMI, an aliasing image, intermodulation distortion, or some other spurious narrowband signal. By themselves, this kind of signal consumes SQUID dynamic range (contributing to nonlinear distortion). When amplified by an incorrectly configured DAN loop, the aggressor signal consumes even more of the SQUID dynamic range, and the DAN loop consumes dynamic range from the nuller DAC and signal chain to do so.

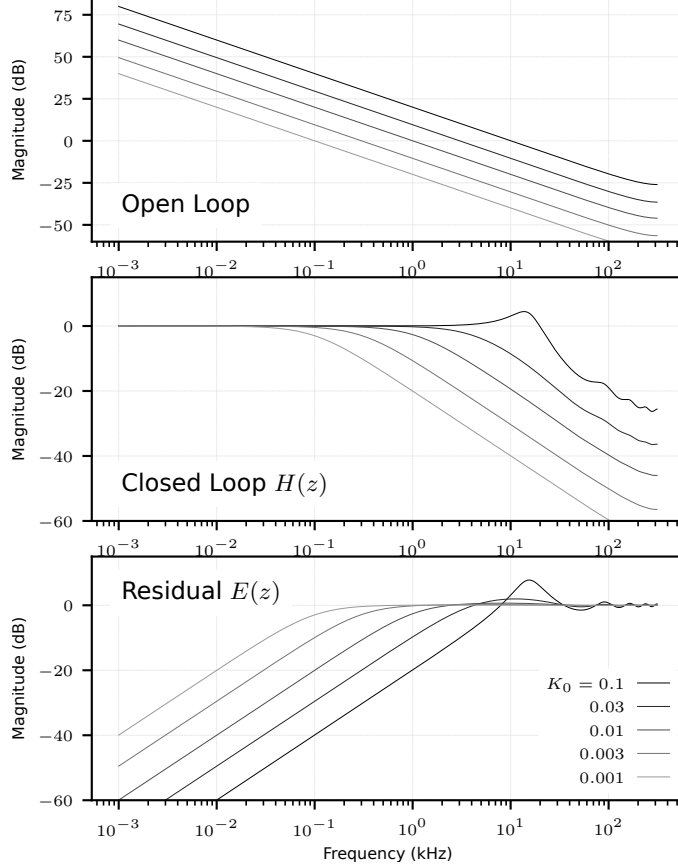


Figure 4. System transfer function vs. frequency, with constant latency $L = 9$ and varying gain K_0 . The gain is varied logarithmically from $K_0 = 10^{-3}$ to $K_0 = 10^{-1}$.

Although we could operate a DAN loop in a region exhibiting peaks, it leaves the feedback loop susceptible to noise sources that are poorly characterized and difficult to control. In a system with many thousands of bolometers at frequencies determined by LC combs that are known to scatter during cooldown, there are likely to be coincidences. Better, then, to choose a loop gain at which this amplification effect is known not to occur.

Figure 6 shows the magnitude and frequency of spectral peaks as a function of loop gain K_0 for latencies $L = 5$, $L = 7$, $L = 9$, and $L = 13$. For each of these latency scenarios, there exist two critical gains K_0 :

- K_{MAX} , beyond which the loop is no longer BIBO stable, and
- K_C , the “critical gain” at which anti-nulling (amplification) starts to occur.

The ratio K_{MAX}/K_C is remarkably independent of latency, and is approximately 3.8 for all latencies between $L = 2$ and $L = 20$.

4. EXPERIMENTALLY DERIVING DAN GAIN

Recall that the combined gain $K_0 = K_N K_D K$, for which we have been evaluating performance, is the product of the nuller gain K_N , demodulator gain K_D , and digital gain K . The nuller and demodulator gains K_N and K_D are themselves products of many gain terms, including terms which are easy to control (amplifier gains, DAC/ADC conversion ratios) and those that are inconvenient to precisely control (cryogenic components, analog filter roll-offs). The uncertainties in these terms compound, leaving an overall system with a great deal of gain variation from bolometer to bolometer on a single SQUID, and from SQUID to SQUID in a larger system.

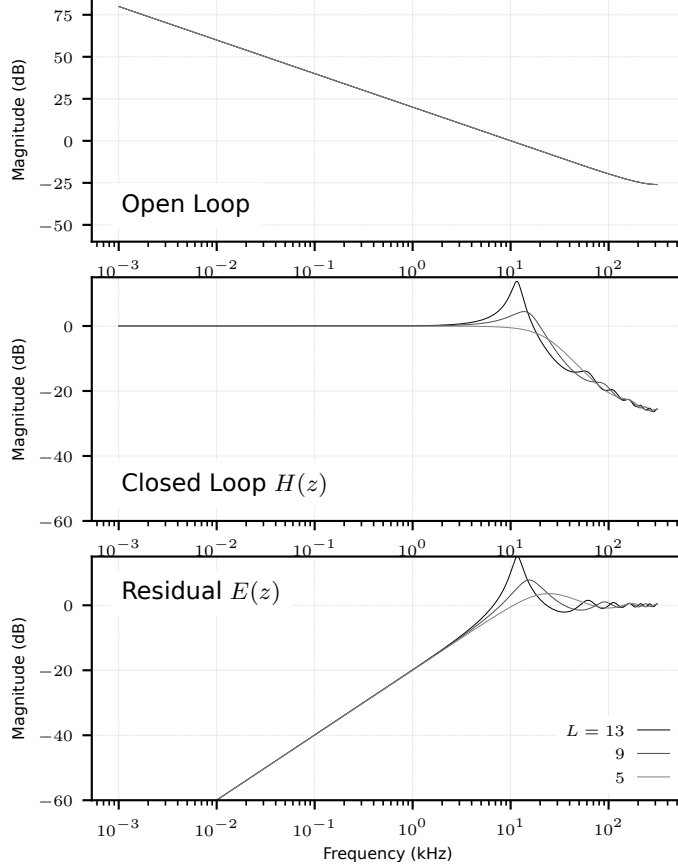


Figure 5. System transfer function vs. frequency, with constant gain $K_0 = 0.1$ and varying latency L .

Although most of these gain terms are fabrication variables and can be measured, the practical complications associated with measuring, tracking, and correctly compensating for these gains are undesirable in an experiment with many thousands of bolometers.

In the past, we accommodated scatter in K_N and K_D by using a digital gain K in the middle of a relatively wide “Goldilocks” region, where nulling efficacy is adequate (even when $K_N K_D$ scatters unexpectedly low) and amplification effects and instabilities have not begun to occur (even when $K_N K_D$ scatters high). As latency increases, however, the size of this Goldilocks region shrinks and we either need to characterize the system better or use another approach.

During the nuller alignment step in the tuning algorithm described above, we injected a fixed nuller signal into the system in order to rotate the nuller phase θ_m^N into anti-alignment with the demodulator (i.e. to correctly establish negative feedback). However, the *magnitude* of the nuller injection gives us a measurement of $K_N K_D$. Hence, we developed the following procedure to establish a consistent loop gain $K_0 < K_C$:

- Choose a desired gain $K_0 < K_C$, e.g. using Figure 6.
- During nuller phase alignment, as described above, a small nuller signal is injected. This causes a complex displacement in the readout signal.
- The angle of this displacement, as described above, is used to determine the nuller phase θ_m^N in order to establish negative feedback.
- The magnitude of this displacement, divided by the amplitude of the nuller probe tone, is a direct measurement of the gain $K_N K_D$. The digital gain parameter K should be set to $K = K_0 / K_N K_D$.

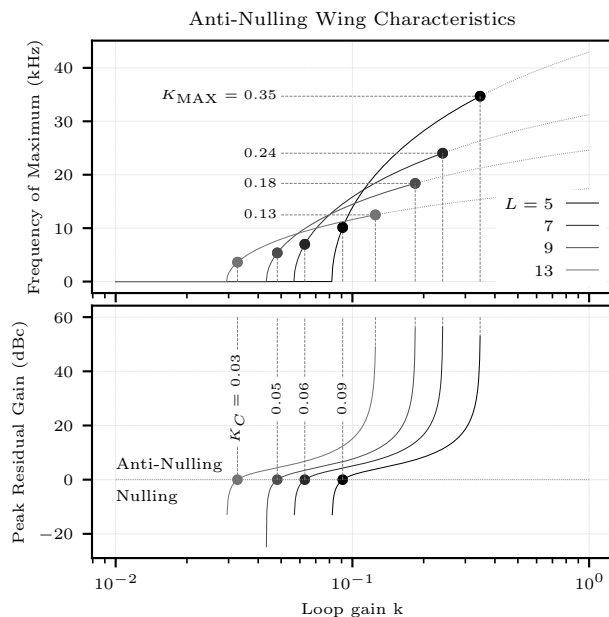


Figure 6. The frequency and gain of spectral peaks in the residual transfer function $E(z)$, as a function of loop gain K_0 . The full range of stable loop gains K_0 is shown; when the loop becomes unstable (i.e. when the poles move outside the unit circle) the line is shown dashed. The maximum BIBO stable gain is marked K_{MAX} for each latency. We also show the critical loop gain K_C for which the wing amplitude (i.e. amplification factor) crosses unity. For effective nulling, the loop gain should never cross this critical gain K_C .

This procedure does not require any additional data capture during tuning, and improves consistency across the system even in systems with low enough latency that detailed gain characterization is unnecessary.

5. CONCLUSIONS

In this paper, we evaluated the effects of latency τ (equivalently, L) on a digital active nulling (DAN) feedback loop used in frequency-multiplexed bolometer readout. We characterized the impact of latency on both BIBO loop stability and the ability to effectively null an input signal.

We found that BIBO-stable gains K_0 between the loop's maximum stable gain K_{MAX} and some critical gain $K_C \approx K_{\text{MAX}}/3.8$ were susceptible to spurious signals within the loop bandwidth, which would be amplified (rather than suppressed) at the SQUID input coil. The frequency of problematic signals depended on both L and K_0 . Although a DAN system can operate above K_C in the absence of aggressor signals, we recommend staying a safe margin below K_C to avoid unpredictable effects in high-bolometer-count systems where spurious signals are not always well characterized, predictable, or controllable.

Finally, we proposed an improved mechanism for determining K to achieve a desired overall loop gain K_0 in the presence of poorly characterized gains K_N, K_D . This tuning step takes advantage of measurements that are already required when establishing phase-aligned negative feedback in the nuller. This procedure compensates for channel-to-channel variability in loop gain due to analog parameter variations (and hence, variability in nulling performance). Loop-gain compensation is desirable even when latency (L, τ) is small enough that the loop performs suitably over a wide enough range of K to accommodate variations in K_N and K_D .

Acknowledgements

The McGill authors acknowledge funding from the Natural Sciences and Engineering Research Council of Canada (NSERC), Canadian Institute for Advanced Research (CIFAR), and Fonds de Recherche Nature et Technologies (FRQNT).

Tijmen de Haan acknowledges the LBNL Chamberlain Fellowship and funding from the Quantum Sensors HEP-QIS Consortium and the LBNL Laboratory Directed Research and Development (LDRD) program under U.S. Department of Energy Contract No. DE-AC02-05CH11231.

REFERENCES

- [1] Bender, A. N., Ade, P. A. R., Ahmed, Z., Anderson, A. J., Avva, J. S., Aylor, K., Barry, P. S., Thakur, R. B., Benson, B. A., Bleem, L. S., Bocquet, S., Byrum, K., Carlstrom, J. E., Carter, F. W., Cecil, T. W., Chang, C. L., Cho, H. M., Cliche, J. F., Crawford, T. M., Cukierman, A., de Haan, T., Denison, E. V., Ding, J., Dobbs, M. A., Dodelson, S., Dutcher, D., Everett, W., Foster, A., Gallicchio, J., Gilbert, A., Groh, J. C., Guns, S. T., Halverson, N. W., Harke-Hosemann, A. H., Harrington, N. L., Henning, J. W., Hilton, G. C., Holder, G. P., Holzappel, W. L., Huang, N., Irwin, K. D., Jeong, O. B., Jonas, M., Jones, A., Khaire, T. S., Knox, L., Kofman, A. M., Korman, M., Kubik, D. L., Kuhlmann, S., Kuo, C. L., Lee, A. T., Leitch, E. M., Lowitz, A. E., Meyer, S. S., Michalik, D., Montgomery, J., Nadolski, A., Natoli, T., Nguyen, H., Noble, G. I., Novosad, V., Padin, S., Pan, Z., Pearson, J., Posada, C. M., Quan, W., Raghunathan, S., Rahlin, A., Reichardt, C. L., Ruhl, J. E., Sayre, J. T., Shirokoff, E., Smecher, G., Sobrin, J. A., Stark, A. A., Story, K. T., Suzuki, A., Thompson, K. L., Tucker, C., Vale, L. R., Vanderlinde, K., Vieira, J. D., Wang, G., Whitehorn, N., Wu, W. L. K., Yefremenko, V., Yoon, K. W., and Young, M. R., “Year two instrument status of the SPT-3G cosmic microwave background receiver,” in [*Millimeter, Submillimeter, and Far-Infrared Detectors and Instrumentation for Astronomy IX*], Zmuidzinas, J. and Gao, J.-R., eds., 2, SPIE (2018).
- [2] Vanderlinde, K., Crawford, T. M., de Haan, T., Dudley, J. P., Shaw, L., Ade, P. A. R., Aird, K. A., Benson, B. A., Bleem, L. E., Brodwin, M., Carlstrom, J. E., Chang, C. L., Crites, A. T., Desai, S., Dobbs, M. A., Foley, R. J., George, E. M., Gladders, M. D., Hall, N. R., Halverson, N. W., High, F. W., Holder, G. P., Holzappel, W. L., Hrubes, J. D., Joy, M., Keisler, R., Knox, L., Lee, A. T., Leitch, E. M., Loehr, A., Lueker, M., Marrone, D. P., McMahan, J. J., Mehl, J., Meyer, S. S., Mohr, J. J., Montroy, T. E., Ngeow, C., Padin, S., Plagge, T., Pryke, C., Reichardt, C. L., Rest, A., Ruel, J., Ruhl, J. E., Schaffer, K. K., Shirokoff, E., Song, J., Spieler, H. G., Stalder, B., Staniszewski, Z., Stark, A. A., Stubbs, C. W., van Engelen, A., Vieira, J. D., Williamson, R., Yang, Y., Zahn, O., and Zenteno, A., “Galaxy Clusters Selected with the Sunyaev-Zel’dovich Effect from 2008 South Pole Telescope Observations,” *Astrophysics Journal* **722**, 1180–1196 (Oct. 2010).
- [3] Schwan, D., Ade, P. A. R., Basu, K., Bender, A. N., Bertoldi, F., Cho, H.-M., Chon, G., Clarke, J., Dobbs, M., Ferrusca, D., Güsten, R., Halverson, N. W., Holzappel, W. L., Horellou, C., Johansson, D., Johnson, B. R., Kennedy, J., Kermish, Z., Kneissl, R., Lanting, T., Lee, A. T., Lueker, M., Mehl, J., Menten, K. M., Muders, D., Pacaud, F., Plagge, T., Reichardt, C. L., Richards, P. L., Schaaf, R., Schilke, P., Sommer, M. W., Spieler, H., Tucker, C., Weiss, A., Westbrook, B., and Zahn, O., “Invited article: Millimeter-wave bolometer array receiver for the Atacama pathfinder experiment Sunyaev-Zel’dovich (APEX-SZ) instrument,” *Review of Scientific Instruments* **82**, 091301 (Sep 2011).
- [4] POLARBEAR Collaboration, “Measurement of the Cosmic Microwave Background Polarization Lensing Power Spectrum with the POLARBEAR experiment,” *Phys. Rev. Lett.* **113**, 021301 (2014).
- [5] Hattori, K., Arnold, K., Barron, D., Dobbs, M., de Haan, T., Harrington, N., Hasegawa, M., Hazumi, M., Holzappel, W. L., Keating, B., Lee, A. T., Morii, H., Myers, M. J., Smecher, G., Suzuki, A., and Tomaru, T., “Adaptation of frequency-domain readout for transition edge sensor bolometers for the POLARBEAR-2 cosmic microwave background experiment,” *Nuclear Instruments and Methods in Physics Research Section A: Accelerators, Spectrometers, Detectors and Associated Equipment* **732**, 299–302 (Dec 2013).
- [6] Bleem, L., Ade, P., Aird, K., Austermann, J., Beall, J., Becker, D., Benson, B., Britton, J., Carlstrom, J., Chang, C. L., Cho, H., de Haan, T., Crawford, T., Crites, A., Datesman, A., Dobbs, M., Everett, W., Ewall-Wice, A., George, E., Halverson, N., Harrington, N., Henning, J., Hilton, G., Holzappel, W., Hoover, S., Hubmayr, J., Irwin, K., Keisler, R., Kennedy, J., Lee, A., Leitch, E., Li, D., Lueker, M., Marrone, D. P., McMahan, J., Mehl, J., Meyer, S., Montgomery, J., Montroy, T., Natoli, T., Nibarger, J., Niemack, M., Novosad, V., Padin, S., Pryke, C., Reichardt, C., Ruhl, J., Saliwanchik, B., Sayre, J., Schafer, K., Shirokoff, E., Story, K., Vanderlinde, K., Vieira, J., Wang, G., Williamson, R., Yefremenko, V., Yoon, K. W., and

- Young, E., “An Overview of the SPTpol Experiment,” *Journal of Low Temperature Physics*, 196 (Jan. 2012).
- [7] Abitbol, M., Aboobaker, A. M., Ade, P., Araujo, D., Aubin, F., Baccigalupi, C., Bao, C., Chapman, D., Didier, J., Dobbs, M., Feeney, S. M., Geach, C., Grainger, W., Hanany, S., Helson, K., Hillbrand, S., Hilton, G., Hubmayr, J., Irwin, K., Jaffe, A., Johnson, B., Jones, T., Klein, J., Korotkov, A., Lee, A., Levinson, L., Limon, M., MacDermid, K., Miller, A. D., Milligan, M., Raach, K., Reichborn-Kjennerud, B., Reintsema, C., Sagiv, I., Smecher, G., Tucker, G. S., Westbrook, B., Young, K., and Zilic, K., “The EBEX balloon-borne experiment—detectors and readout,” *The Astrophysical Journal Supplement Series* **239**, 8 (Nov 2018).
- [8] Irwin, K., Nam, S., Cabrera, B., Chugg, B., Park, G., Welty, R., and Martinis, J., “A self-biasing cryogenic particle detector utilizing electrothermal feedback and a SQUID readout,” *IEEE Transactions on Applied Superconductivity* **5**, 2690–2693 (June 1995).
- [9] Lanting, T., Cho, H.-M., Clarke, J., Dobbs, M., Holzapfel, W., Lee, A., Lueker, M., Richards, P., Smith, A., and Spieler, H., “Frequency-domain SQUID multiplexing of transition-edge sensors,” *IEEE Transactions on Applied Superconductivity* **15**, 567–570 (Jun 2005).
- [10] Smecher, G., Aubin, F., Bissonnette, E., Dobbs, M., Hyland, P., and MacDermid, K., “A biasing and demodulation system for kilopixel TES bolometer arrays,” *IEEE Transactions on Instrumentation and Measurement* **61**, 251–260 (Jan 2012).
- [11] de Haan, T., Smecher, G., and Dobbs, M., “Improved performance of TES bolometers using digital feedback,” in [*Society of Photo-Optical Instrumentation Engineers (SPIE) Conference Series*], *Society of Photo-Optical Instrumentation Engineers (SPIE) Conference Series* **8452** (Sept. 2012).
- [12] Tomaru, T., Hazumi, M., Lee, A. T., Ade, P., Arnold, K., Barron, D., Borrill, J., Chapman, S., Chinone, Y., Dobbs, M., Errard, J., Fabbian, G., Ghribi, A., Grainger, W., Halverson, N., Hasegawa, M., Hattori, K., Holzapfel, W. L., Inoue, Y., Ishii, S., Kaneko, Y., Keating, B., Kermish, Z., Kimura, N., Kisner, T., Kranz, W., Matsuda, F., Matsumura, T., Morii, H., Myers, M. J., Nishino, H., Okamura, T., Quealy, E., Reichardt, C. L., Richards, P. L., Rosen, D., Ross, C., Shimizu, A., Sholl, M., Siritanasak, P., Smith, P., Stebor, N., Stompor, R., Suzuki, A., Suzuki, J.-i., Takada, S., Tanaka, K.-i., and Zahn, O., “The POLARBEAR-2 experiment,” in [*Society of Photo-Optical Instrumentation Engineers (SPIE) Conference Series*], *Society of Photo-Optical Instrumentation Engineers (SPIE) Conference Series* **8452**, 1 (Sept. 2012).
- [13] Lowitz, A. E., Bender, A. N., Dobbs, M. A., and Gilbert, A., “Digital frequency multiplexing with sub-kelvin SQUIDS,” in [*Millimeter, Submillimeter, and Far-Infrared Detectors and Instrumentation for Astronomy IX*], Zmuidzinas, J. and Gao, J.-R., eds., SPIE (Jul 2018).
- [14] Harris, F. J., [*Multirate Signal Processing for Communication Systems*], Prentice Hall (2004).